crystals

MDPI

Article

Thermal Regulation of the Acoustic Bandgap in Pentamode Metamaterials

Jing Cheng [1], Shujun Liang [2] and Yangyang Chu [2,*]

[1] Engineering Training Center, Zhengzhou University of Light Industry, Zhengzhou 450001, China; 2019069@zzuli.edu.cn
[2] College of Software Engineering, Zhengzhou University of Light Industry, Zhengzhou 450001, China; liangsj@zzuli.edu.cn
* Correspondence: chuyang@zzuli.edu.cn

Abstract: This study used the finite element method to investigate the acoustic bandgap (ABG) characteristics of three-dimensional pentamode metamaterial (PM) structures under the thermal environment, and a method for controlling the PM ABG based on external temperature variation is also proposed. The results indicate that the complete acoustic bandgap can be obtained for a PM in the thermal environment, which makes the PM combine the bandgap characteristics of phononic crystals. More than that, the bandwidth and locations of ABGs can be effectively manipulated by controlling the temperature. Considering the softening effect of thermal stresses, the ABG gradually moves to lower frequencies as the temperature increases. Based on this, different degrees of ABG tunability can be achieved by changing the thermal environment to propagate or suppress acoustic waves of different frequencies. This work provides the possibility for PMs to realize intelligent regulation of the bandgap.

Keywords: acoustic bandgap; petamode metamaterial; thermal environment; bandwidth

Citation: Cheng, J.; Liang, S.; Chu, Y. Thermal Regulation of the Acoustic Bandgap in Pentamode Metamaterials. *Crystals* **2024**, *14*, 992. https://doi.org/10.3390/cryst14110992

Academic Editor: Luis M. Garcia-Raffi

Received: 23 October 2024
Revised: 15 November 2024
Accepted: 15 November 2024
Published: 17 November 2024

1. Introduction

Phononic crystals are artificial periodic composite materials or structures with the unique property of prohibiting the propagation of elastic waves within certain frequency ranges [1,2]. Furthermore, if the unit configuration of phononic crystals is designed to the sub-wavelength scale through artificial microstructure design, the propagation of elastic waves can be modulated through the local resonance effect, which is accompanied by some novel effects that natural materials do not possess; this kind of structural material is referred to as acoustic metamaterials. Due to its unique physical properties, it has promising applications in the fields of acoustic absorption [3,4], sound stealth [5,6], acoustic communication [7], and other fields.

PM is a novel acoustic/elastic metamaterial structure suggested by Milton and Cherkaev [8], which is gradually becoming known by its solid structural features and fluid properties. PMs have advantages such as broadband effectiveness, solid morphology, and diverse selection of matrix media, and the effective parameters of PMs depend on their substrate parameters and microstructure geometry, which can be adjusted simultaneously or independently to change their effective parameters. Therefore, the equivalent parameters of a PM can be changed by designing the microstructure and changing the size or shape of the microstructure. Norris [9] theoretically analyzed the feasibility of PMs for acoustic cloaks. Chen [10] designed an aluminum-based PM acoustic metasurface invisibility cloak using a hierarchical optimization algorithm and performed acoustic–solid coupling numerical simulations of the microstructure, which confirmed its broad low-frequency acoustic stealth performance. The conventional PM is a diamond-type structure consisting of 16 double-cone elements, which exhibit good symmetry. Such PM structures have only single-mode regions where compression waves

are propagated and shear waves are suppressed, and there is no complete acoustic bandgap. In previous studies of phononic crystals, the degeneracy of energy bands at high symmetry points in the Brillouin region could be removed by reducing lattice symmetry [11]. Wang et al. [12] broke the symmetry of the structure by introducing geometrical perturbations in a PM, and a complete phonon bandgap was obtained in addition to the single-mode frequency region. In this way, such PMs not only have an anisotropic elastic modulus but also possess the bandgap characteristics of phononic crystals. Based on the principle of local resonance, a PM composed of composite materials was proposed and investigated [13], which offers the possibility for PMs to be used for low-frequency acoustic wave modulation. Zou et al. [14] proposed several novel curved PMs by modifying the straight sides of conventional PMs with curves and further improved the bandgap characteristics of the proposed PM through multi-objective optimization research. Zhao et al. [15] designed a unique underwater multiphase microstructure that can simultaneously operate the wavefront and sound absorption, which can significantly improve acoustic stealth capability.

Previous studies obtained the complete phonon bandgap by introducing structural perturbations into the PM structure to break the symmetry of the original structure and then widening and changing the complete phonon bandgap by increasing the asymmetry [16]. But for a given PM structure, once the structure is molded, its acoustic properties are virtually unchangeable. Moreover, how to obtain a complete phonon bandgap without changing the PM structure and effectively regulating it has not been studied yet. In addition, it is worth mentioning that PM structures are used in thermal environments taking into account the thermal effect, which changes the elastic constants of the materials, causes thermal deformation of the structure, and generates thermal stresses, bringing unprecedented challenges to the study of vibration and noise reduction control methods in thermal environments.

To obtain tunable bandgap structures, many smart materials such as piezoelectric [17–19], contact [20], conformationally altered [21], flexural [22,23], and thermal [24–27] constituting acoustic metamaterials have gained the attention of many scholars at home and abroad. Therefore, with the idea of intelligent materials, the bandgap characteristics of PMs can be adjusted by temperature change, thus providing the possibility of bandgap tunability of PMs without changing the structure.

This article aims to utilize the thermal environment to obtain and manipulate the bandgap in PM structures. The main reasons for the generation of bandgap are discussed. Considering the softening effect of thermal stresses, the bandgap properties of the lattice structure at different temperatures are calculated by the finite element method. Changing the thermal environment to propagate or inhibit the sound waves of different frequencies provides some references for the acoustic modulation of PM structures and the intelligent control of bandgaps.

2. Band Structure of a PM in the Thermal Environment

In this paper, a composite PM (CPM) structure based on the PM structure proposed by Kadic [28] is considered to study its effect on the band structure in the thermal environment. The CPM structure is composed of 16 double-cone elements, each pair of cones being interconnected by a wide diameter D to constitute a double-cone unit. The double-cone units are interconnected by contacts at their narrow diameters d, forming a face-centered cubic structure with lattice constant a, as illustrated in Figure 1. The height of a double-cone unit can be expressed as $H = \sqrt{3}a/4$. In this paper, the structural parameters are fixed as a = 37.3 mm, D = 3 mm, d = 0.55 mm, and $h = 0.04H$. The PM structure consists of two different materials: aluminum (gray area) and silicone rubber (black area). The material parameters used in this paper are shown in Table 1. Since aluminum is a temperature-dependent material, its parametric model can be expressed as [29]:

$$P = P_0\left(P_{-1}T^{-1} + 1 + P_1T + P_2T^2 + P_3T^3\right) \quad (1)$$

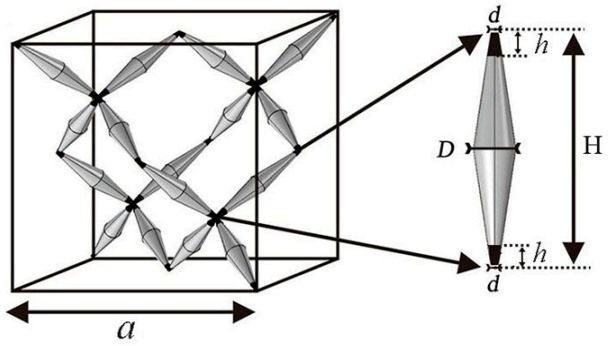

Figure 1. Schematic illustration of the PM structure.

Table 1. Material parameters of the PM.

Material	Yong's Modulus, E (Pa)	Mass Density, ρ (kg/m^3)	Poissom's Ration, ν	Thermal Expansion Coefficient, α (1/K)
Aluminum	E_1	2730	0.352	α_1
Silicon rubber	1.37×10^5	1300	0.464	5.9×10^{-4}

Table 2 lists P_0, P_{-1}, P_1, $P_{2,}$ and P_3 for the temperature coefficients, and T (K) is the temperature field. The temperatures considered for the calculations in this paper are not high, so the other material parameters are set as constants during the calculations.

Table 2. Aluminum material characteristic coefficients with temperature.

Material	P_{-1}	P_0	P_1	P_2	P_3
E (Gpa)	0	200	-4.5853×10^{-3}	1.0498×10^{-5}	-8.3375×10^{-9}
A (1/K)	0	15.416×10^{-6}	1.6175×10^{-3}	-4.5283×10^{-7}	0

Using 3D CAD software to establish a coordinate system with the center of the face-centered cubic lattice as the coordinate origin, the single-cell model was constructed based on the above geometric parameters. Then, the band structure of the PM was numerically analyzed using the finite element method. The model was established, and Bloch periodic boundary conditions were applied. A free tetrahedral mesh to partition the primitive cells, with a degree of freedom of 187,341, a maximum cell growth rate of 1.5, a curvature resolution of 0.6, and a narrow region resolution of 0.5, was used to ensure the convergence of the calculation results. By scanning the wave vector k along the first irreducible Brillouin zone high symmetry point (ΓXWLΓK) to solve the elastic dynamics equation, the eigenfrequencies were calculated.

The band structure of the PM at 40 °C was calculated, as illustrated in Figure 2b. For comparison, the PM at room temperature (i.e., 20 °C, with no temperature field applied) was also calculated, as demonstrated in Figure 2a. Only the first 20 orders of dispersion curves are plotted. It is observed that at room temperature, only the single-mode frequency region of the PM exists and there is no complete acoustic bandgap that can suppress all acoustic wave transmission. As illustrated in Figure 2b, the band structure of the PM is relatively compressed in the thermal environment compared to the room environment. In addition, a complete acoustic bandgap (light yellow region) is obtained in the frequency range from 861.9 to 1113.0 Hz, in which all acoustic waves can be isolated. Thus, by varying the temperature, it has not only the single-mode bandgap characteristics but also the low-frequency ABG properties of locally resonant phononic crystals. In the range of single-mode bandgaps, the PM has fluid properties. In thermal environments, all acoustic waves cannot be transmitted over the complete ABG, and the PM has acoustic isolation properties.

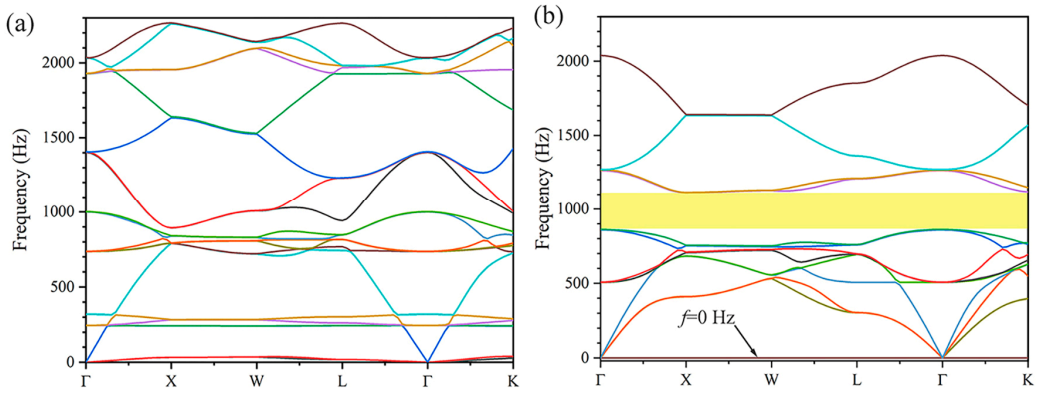

Figure 2. The band structure of the PM at (**a**) room temperature and (**b**) at 40 °C.

3. Analysis of Factors Affecting Bandgap Generation

Then, the reasons why the PM obtains a complete acoustic bandgap in the thermal environment were analyzed. For elastic structures, each part of the elastomer in the thermal environment generally expands with increasing temperature. In addition, the thermal environment can change the material properties of the structure and can also cause thermal deformation of the structure, resulting in thermal stresses. Therefore, the effect of combined thermal stress and temperature-dependent material properties on the band structure of the PM was explored. The band structure was investigated separately for three different cases, i.e., at room temperature, considering only thermal stresses, and the coupling effect of thermal stresses with temperature-dependent material, as shown in Figure 3. The band structure of PM at 40 °C is very different from that at room temperature. It is clear from the figure that a complete acoustic bandgap appears when only thermal stresses are considered. Moreover, the influence of coupling effects slightly reduces the frequency values compared to considering only thermal stress effects, as shown in Figure 3b. However, the coupling is of limited significance, probably due to the small change in the elastic modulus of aluminum as the temperature rises to 40 °C. Therefore, thermal stress plays a major role in influencing the band structure as a key factor in the generation of bandgaps when temperature is not too high.

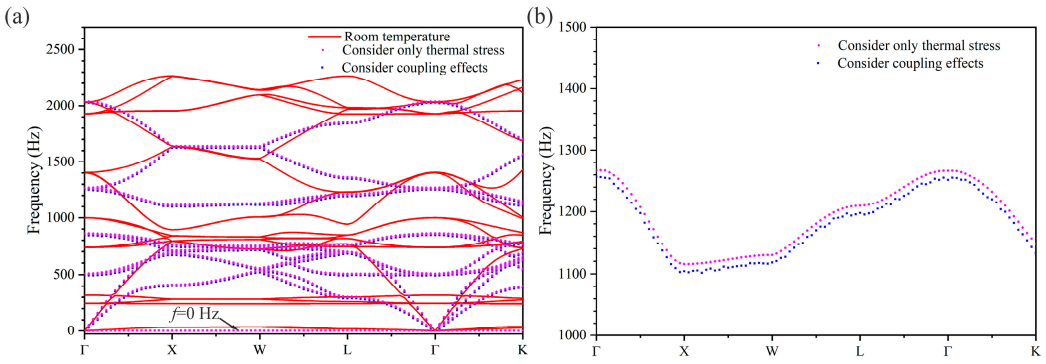

Figure 3. The band structure of the PM is affected by different factors. (**a**) Band structures. (**b**) Localized diagrams of the two bands. The red curve indicates the bandgap structure at room temperature. Pink dotted lines indicate that only thermal stresses are affected at 40 °C. The blue dotted line indicates the influence of both thermal stresses and thermally variable materials at 40 °C.

4. Bandgap Manipulation by the Thermal Environment

4.1. Distribution of Thermal Stresses in the PM

Thermal stress is the main factor affecting the band structure, and its distribution in the PM structure was further analyzed. When the temperature changes, the PM is subjected to external confinement effects and mutual restraining effects between the internal constituent

structures, expansion cannot occur freely, and thermal stresses will be generated. Figure 4 shows the thermal stress distribution of the PM at 40 °C. It can be observed that the normal stress in the x-direction is much greater than the shear stress component. The fact that silicone rubber is softer and less stiff than aluminum material prevents the expansion of the aluminum from being hindered, resulting in normal stresses concentrated mainly in the aluminum structure. However, the shear stresses arise mainly at the interface between them due to the mismatch in their thermal expansion, whereas the shear component of the thermal stresses is zero in a homogeneous isotropic material.

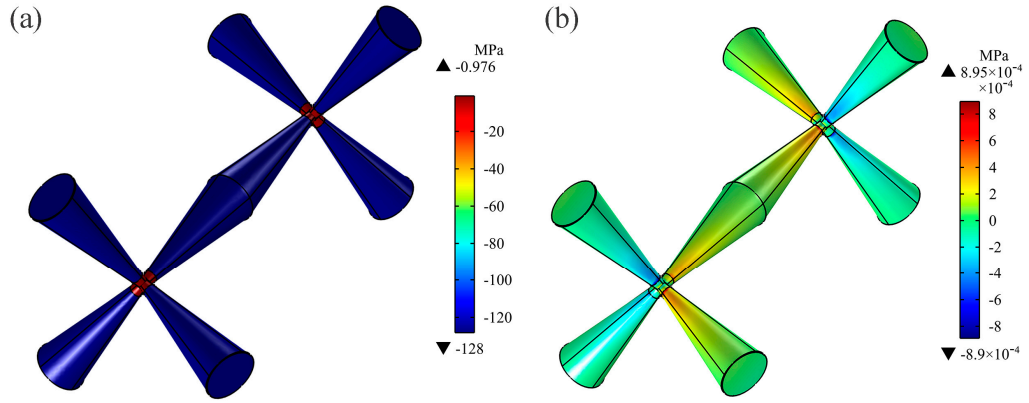

Figure 4. The thermal stress distribution of the PM in 40 °C. Unit: N/m^2. (**a**) Normal thermal stresses in the *x*-direction. (**b**) Shear thermal stresses.

4.2. Effect of Thermal Stress on the Band Structure

Figure 5 illustrates the band structure of the PM subjected to thermal stress at different temperatures, and the three colored curves in the figure are the band structures in different thermal environments. It can be easily seen that there is a complete acoustic bandgap in the band structure, and all the band curves show a downward trend with increasing temperature. According to the stress distribution in Figure 4, the normal thermal stress is negative, while the shear thermal stress has not only positive but also negative values, but its magnitude is much smaller than the normal thermal stress. This will reduce the stiffness of the PM structure, causing the band curve to shift towards low frequencies. The bandgap frequency range varied from 935.9–1190.3 Hz (30 °C) to 775.7–1027.4 Hz at 50 °C. Thus, thermal stresses can modulate the ABG.

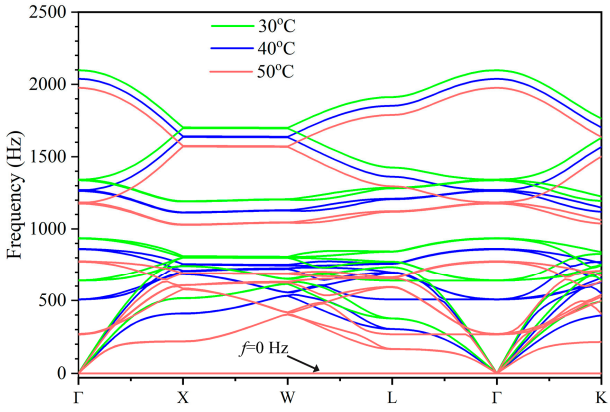

Figure 5. Variation in the band structure with temperature.

From the vibration theory, the modal parameters of the PM can be obtained with the below formula.

$$\left(\mathbf{K} - \omega^2 \mathbf{M}\right) \mathrm{U} = 0 \tag{2}$$

where K is the total structural stiffness matrix, M is the mass matrix, and U is the vibration mode vector. When the PM structure is in a thermal environment, the variation in the mass matrix M is ignored, while the influence of thermal stresses induced by the thermal environment on the stiffness matrix needs to be considered. Therefore, the total stiffness matrix K of the PM under thermal environment conditions can be written as:

$$\mathbf{K} = \mathbf{K}_T + \mathbf{K}_\sigma \tag{3}$$

where $\mathbf{K}_T$ is the structural stiffness matrix and $\mathbf{K}_\sigma$ is the thermal stress stiffness matrix.

In Equation (3), matrix $\mathbf{K}_T$ is associated with the physical properties of the PM. The thermal stress stiffness matrix $\mathbf{K}_\sigma$ has a close relationship with the thermal stress form in the PM. When the thermal stress $\mathbf{K}_\sigma$ is positive, the natural frequency of the structure tends to increase, and, on the contrary, the intrinsic frequency moves to lower frequencies.

From Figure 4a, it can be seen that the thermal stress at 40 °C is negative and hence the eigenfrequency converges to decrease, which is in accordance with the trend of the bandgap structure with temperature in Figure 5. Therefore, the bandgap structure of the PM can be effectively regulated by temperature.

It is noteworthy that in Figures 2b, 3a and 5, zero-frequency bands appear in the low-frequency bands as thermal stress is applied. This is because the structural stiffness of the PM is less than the additional negative thermal stress stiffness under the wave vector condition in the central Brillouin zone, resulting in the stiffness matrix becoming indefinite. In addition, the corresponding imaginary frequencies also appear in the zero-frequency bands. Figure 6 depicts the band structure of the imaginary frequency and real wave number at different temperatures. As the temperature increases, the amplitude of the imaginary frequency increases. Usually free-wave transmission is considered only when the wave vector is real, and the occurrence of imaginary frequencies may be related to the attenuation of free fluctuations [30]. In addition, reference [31] shows that a larger imaginary frequency amplitude implies a larger free fluctuation attenuation and narrower bandgap, which is consistent with the research conclusion of this paper.

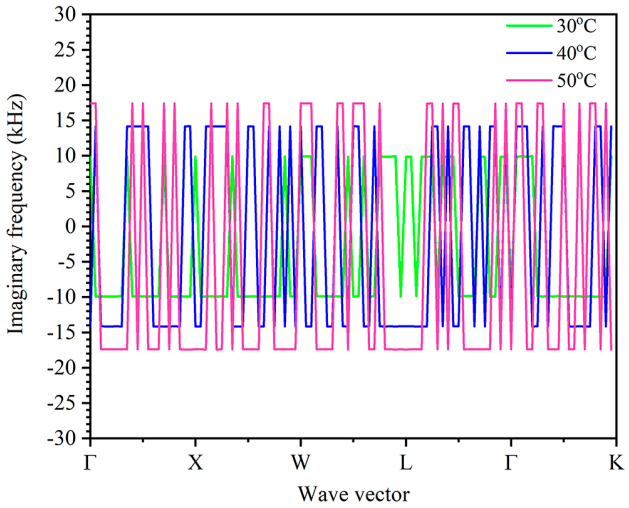

Figure 6. The band structure of the imaginary frequency and real wave number at different temperatures.

4.3. The Bandgap Manipulation by the Thermal Environment

Then, the thermal environment effect on the ABG characteristics of PM was investigated. Figure 7 displays the variation in the ABG with temperature. The calculations show that both the upper and lower bound frequencies of the ABG drift to lower frequencies as temperature increases. The frequency range of the bandgap decreases from 972.6 Hz–1236.8 Hz to 253.5 Hz–384.4 Hz as the temperature increases from 25 °C to 80 °C.

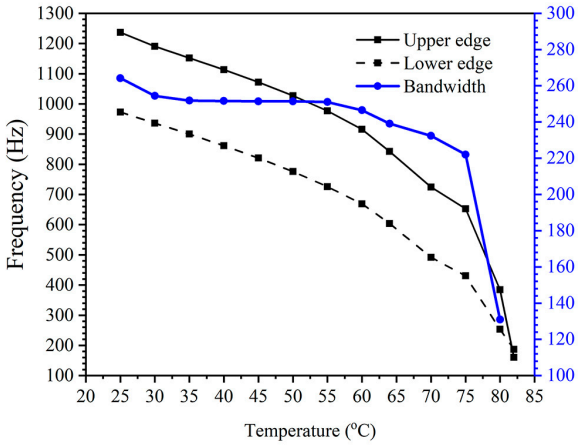

Figure 7. The trend of the complete bandgap with temperature.

In addition, Figure 7 shows the variation in the bandgap width with temperature. The bandwidth gradually decreases from 264.2 Hz to 130.9 Hz as the temperature changes from 25 °C to 80 °C. It should be notable that the ABG is more insensitive to temperature at higher frequencies, and it disappears at 82 °C. The bandwidth decreases slightly as the temperature increases from 25 °C to 75 °C. However, as the temperature rises from 75 °C to 82 °C, the bandwidth drops dramatically from 222 Hz until it disappears. This may be the result of localized instability caused by the thermal buckling effect on the PM structure when the temperature is too high. These results show that when using a PM for vibration and wave propagation control in the thermal environment, temperature changes can be utilized to efficiently modulate the bandwidth and achieve control of the bandgap position and opening/closing.

5. Conclusions

In this study, the variation in the band structure and the ABG for a PM in the thermal environment are investigated by numerical methods. The simulation results show that the PM obtains a complete acoustic bandgap when the temperature changes, exhibiting the bandgap characteristics of phononic crystals. The effects of the changing factors on the band structure in thermal environments are further investigated, and the results show that thermal stress is the main factor in the generation of the bandgap. Considering the thermal stress, the lower and upper frequencies of the complete bandgap will move to the lower frequency as the temperature rises, and the bandgap will be narrowed until it disappears. The research results in this paper can guide the design of PM vibration and noise reduction in thermal environments and can also be used to flexibly control and direct underwater acoustic waves, which is promising for applications in marine communications.

Author Contributions: Writing—original draft, J.C.; writing—review and editing, S.L.; methodology, Y.C. All authors have read and agreed to the published version of the manuscript.

Funding: This research received no funding.

Data Availability Statement: The original contributions presented in this study are included in this article material. Further inquiries can be directed to the corresponding author.

Conflicts of Interest: The authors declare no conflicts of interest.

References

1. Sigalas, M.M.; Economou, E.N. Elastic and acoustic wave band structure. *J. Sound Vib.* **1992**, *158*, 377–382. [CrossRef]
2. Kushwaha, M.S.; Halevi, P.; Dobrzynski, L.; Djafari-Rouhani, B. Acoustic band structure of periodic elastic composites. *Phys. Rev. Lett.* **1993**, *71*, 2022–2025. [CrossRef] [PubMed]
3. Wang, T.; Chen, M.; Dong, W.; Guo, H. Low-frequency sound and vibration reduction of a metamaterial plate submerged in water. *Eur. J. Mech. A-Solids* **2022**, *96*, 104764. [CrossRef]

4. Chen, D.; Zi, H.; Li, Y.; Li, X. Low frequency ship vibration isolation using the band gap concept of sandwich plate-type elastic metastructures. *Ocean Eng.* **2021**, *235*, 109460. [CrossRef]
5. Mendez, C.G.; Podesta, J.M.; Lloberas-Valls, O.; Toro, S.; Huespe, A.E.; Oliver, J. Computational material design for acoustic cloaking. *Int. J. Numer. Methods Eng.* **2017**, *112*, 1353–1380. [CrossRef]
6. Matsushima, K.; Noguchi, Y.; Yamada, T. Omnidirectional acoustic cloaking against airborne sound realized by a locally resonant sonic material. *Sci. Rep.* **2022**, *12*, 16383. [CrossRef]
7. Bok, E.; Park, J.J.; Choi, H.; Han, C.K.; Wright, O.B.; Lee, S.H. Metasurface for Water-to-Air Sound Transmission. *Phys. Rev. Lett.* **2018**, *120*, 044302. [CrossRef]
8. Milton, G.W.; Cherkaev, A.V. Which Elasticity Tensors are Realizable? *J. Eng. Mater. Technol.* **1995**, *117*, 483–493. [CrossRef]
9. Norris, A.N. Acoustic cloaking theory. *Proc. R. Soc. A-Math. Phys. Eng. Sci.* **2008**, *464*, 2411–2434. [CrossRef]
10. Chen, Y.; Liu, X.; Hu, G. Latticed pentamode acoustic cloak. *Sci. Rep.* **2015**, *7*, 5. [CrossRef]
11. Caballero, D.; Sanchez-Dehesa, J.; Rubio, C.; Mártinez-Sala, R.; Sánchez-Pérez, J.V.; Meseguer, F.; Llinares, J. Large two-dimensional sonic band gaps. *Phys. Rev. E* **2000**, *60*, R6316. [CrossRef] [PubMed]
12. Cai, C.X.; Wang, Z.H.; Li, Q.W.; Xu, Z.; Tian, X.G. Pentamode metamaterials with asymmetric double-cone elements. *J. Phys. D-Appl. Phys.* **2015**, *48*, 175103. [CrossRef]
13. Wang, Z.; Chu, Y.; Cai, C.; Liu, G.; Wang, M.R. Composite pentamode metamaterials with low frequency locally resonant characteristics. *J. Appl. Phys.* **2017**, *122*, 025114. [CrossRef]
14. Zou, Z.; Xu, F.; Pan, Y.; Fang, T. Bandgap properties and multi-objective optimization of double-cone pentamode metamaterials with curved side. *Phys. Scr.* **2023**, *98*, 035833. [CrossRef]
15. Chu, Y.Y.; Li, Y.C.; Cai, C.X.; Liu, G.S.; Wang, Z.H.; Xu, Z. Ultrawide bandgap pentamode metamaterials with an asymmetric double-cone outside profile. *J. Phys. D-Appl. Phys.* **2018**, *51*, 125103. [CrossRef]
16. An, Y.; Zou, H.; Zhao, A. Broadband Waterborne Multiphase Pentamode Metastructure with Simultaneous Wavefront Manipulation and Energy Absorption Capabilities. *Materials* **2023**, *16*, 5051. [CrossRef]
17. Casadei, F.; Delpero, T.; Bergamini, A.; Ermanni, P.; Ruzzene, M. Piezoelectric resonator arrays for tunable acoustic waveguides and metamaterials. *J. Appl. Phys.* **2012**, *112*, 064902. [CrossRef]
18. Bacigalupo, A.; De Bellis, M.L.; Misseroni, D. Design of tunable acoustic metamaterials with periodic piezoelectric microstructure. *Extrem. Mech. Lett.* **2020**, *40*, 100977. [CrossRef]
19. Huang, Z.-G. Silicon-based filters, resonators and acoustic channels with phononic crystal structures. *J. Phys. D-Appl. Phys.* **2011**, *44*, 245406. [CrossRef]
20. Kim, E.; Martinez, A.J.; Phenisee, S.E.; Kevrekidis, P.G.; Porter, M.A.; Yang, J. Direct measurement of superdiffusive energy transport in disordered granular chains. *Nat. Commun.* **2018**, *9*, 640. [CrossRef]
21. Liu, Y.; Sun, X.-Z.; Jiang, W.-Z.; Gu, Y. Tuning of Bandgap Structures in Three-Dimensional Kagome-Sphere Lattice. *J. Vib. Acoust.* **2014**, *136*, 021016. [CrossRef]
22. Li, Z.; Li, Y.; Kumar, S.; Lee, H.P. Thermal tuning of negative effective mass density in a two-dimensional acoustic metamaterial with hexagonal lattice. *J. Appl. Phys.* **2019**, *126*, 155102. [CrossRef]
23. Khanikaev, A.B.; Fleury, R.; Mousavi, S.H.; Alu, A. Topologically robust sound propagation in an angular-momentum-biased graphene-like resonator lattice. *Nat. Commun.* **2015**, *6*, 8260. [CrossRef] [PubMed]
24. Sun, Y.; Xiao, Y.; Vignali, V. Acoustic Radiation Performance of a Composite Laminated Plate Subjected to Local Temperature. *Adv. Civ. Eng.* **2022**, *2022*, 9912765. [CrossRef]
25. Zhao, Z.; Cui, X.B.; Yin, Y.F.; Li, Y.H.; Li, M. Thermal tuning of vibration band gaps in homogenous metamaterial plate. *Int. J. Mech. Sci.* **2022**, *225*, 107374. [CrossRef]
26. Martin, A.; Kadic, M.; Schittny, R.; Bückmann, T.; Wegener, M. Phonon band structures of three-dimensional pentamode metamaterials. *Phys. Rev. E* **2012**, *86*, 4172–4181. [CrossRef]
27. Yue, H.B.; Wang, W.; Xu, W.K.; Yuan, S.S. Band Gap Characteristics of Planar Stretch-Dominated Thermal Expansion Lattice Metamaterial. *Acta Phys. Pol. A* **2021**, *140*, 438–444. [CrossRef]
28. Lv, S.C.; Xu, W.K.; Bai, L.; Qi, W.C.; Wang, W. Thermal tuning of band gap properties in planar stretch-dominated lattices with tailorable coefficient of thermal expansion. *Appl. Phys. A-Mater. Sci. Process* **2021**, *127*, 425. [CrossRef]
29. Han, J.; Yu, K.; Li, X.; Zhao, R. Modal density and mode counts of sandwich panels in thermal environments. *Compos. Struct.* **2016**, *153*, 69–80. [CrossRef]
30. Frazier, M.J.; Hussein, M.I. Generalized Bloch's theorem for viscous metamaterials: Dispersion and effective properties based on frequencies and wavenumbers that are simultaneously complex. *Comptes Rendus Phys.* **2016**, *17*, 565–577. [CrossRef]
31. Wu, J.H.; Liu, A.Q.; Ang, L.K.; Cheng, T.H.; Xu, K.; Wu, J.; Lin, J.T. Complex photonic band diagrams for finite-size photonic crystals with arbitrary defects. *J. Appl. Phys.* **2007**, *101*, 053101. [CrossRef]